TITLE:

# Interference effects in high-order harmonics from colloidal perovskite nanocrystals excited by an elliptically polarized laser

AUTHOR(S):

Nakagawa, Kotaro; Hirori, Hideki; Sanari, Yasuyuki; Sekiguchi, Fumiya; Sato, Ryota; Saruyama, Masaki; Teranishi, Toshiharu; Kanemitsu, Yoshihiko

# Interference effects in high-order harmonics from colloidal perovskite nanocrystals excited by an elliptically polarized laser

Kotaro Nakagawa, Hideki Hirori [*], Yasuyuki Sanari, Fumiya Sekiguchi, Ryota Sato, Masaki Saruyama,
Toshiharu Teranishi, and Yoshihiko Kanemitsu [†]

*Institute for Chemical Research, Kyoto University, Uji, Kyoto 611-0011, Japan*

Halide perovskite nanocrystals are suitable materials for photonic devices because their highly efficient luminescence can be tuned over a wide wavelength range by changing the nanocrystal composition and size. Here, we report on the high-order harmonic generation in a solution-processed perovskite $CsPbBr_3$ nanocrystal film that is excited by a strong midinfrared laser. We observe harmonics up to the 13th order, which is ultraviolet light well above the band-gap energy. By using elliptically polarized laser light, we analyze the influence of the sample structure on the intensity of the 5th harmonic. It is also found that the randomness in the orientation of the nanocrystals in the film induces a reduction in the harmonic intensities due to the interference among the harmonics emitted from nanocrystals with different phases. Our observation of high-order harmonics from nanocrystal films opens a way towards the development of an intensity modulator that can be tuned simply by changing the excitation ellipticity.

DOI: [10.1103/PhysRevMaterials.5.016001](10.1103/PhysRevMaterials.5.016001)

## I. INTRODUCTION

Lead halide perovskites have been attracting much attention as device materials for solar cells, optical detectors, light-emitting diodes, lasers, optical modulators, etc. [1–13]. These materials are promising alternatives to the conventional but rather expensive semiconductor device materials, because high-quality perovskite crystals with extremely low defect densities can be fabricated using simple and low-cost chemical solution processes [1–3]. In addition to the optical, electrical, and thermal properties of halide perovskite single crystals and thin films [14–19], the unique optical properties of perovskite nanocrystals (NCs) have recently also started to attract attention [20–25]. A very high emission efficiency (>80%) can be obtained from these NCs even without using special surface passivation methods, and by changing the NC composition and size, emission at any wavelength in the visible region can be achieved. Furthermore, perovskite NCs can enhance the optical responses by excitonic quantum confinement, which makes the perovskite NCs attractive from the viewpoint of nonlinear materials [26–28].

While the generation of band-edge emission is sufficient for many applications, second harmonic generation and similar phenomena can significantly extend the range of accessible wavelengths. High-order harmonic generation (HHG) is a nonperturbative nonlinear optical phenomenon caused by excitation with strong laser fields. Note that HHG is different from conventional perturbative phenomena like second or third harmonic generation, and it is considered useful for bright extreme ultraviolet (XUV) sources and

attosecond laser technologies [29,30]. HHG was first discovered in gases [29,31]. The discovery of HHG in solids is considered important for the development of compact and efficient optoelectronic HHG devices because of the higher electron density available in solids and easier handling [32,33]. To advance HHG applications, much effort has been devoted to elucidating the HHG mechanism in solids. So far, various different materials including different forms such as bulk materials, amorphous materials, films, and single atomic layers, have been considered in research on HHG [32–40]. However, studies on HHG in NCs, which have unique electronic structures different from the discrete levels in atoms and the continuous states in solids [41–43], are still lacking. Defect-tolerant halide perovskite NCs are suitable for studying HHG, because extremely low densities of defects within the band-gap enable us to clarify the roles of the intrinsic electronic states. Besides the fundamental physics of HHG, practical aspects should be considered as well. As the efficiencies of HHG in halide perovskites can compete with those in typical materials for HHG such as GaSe, low-cost thin films of high-quality perovskite NCs may be a practically important material for HHG.

In this study, we observed high-order harmonics (HHs) from a film of colloidal lead halide perovskite $CsPbBr_3$ NCs with a particle size of 10 nm. In our experiments, harmonics up to the 13th order (which is well above the band-gap energy) were observed when the NC film was excited by a strong midinfrared laser with linear polarization. We also varied the excitation polarization and compared the obtained HH intensities of the $CsPbBr_3$ NC film and $MAPbCl_3$ bulk single crystal (SC). The HH intensity of the NC ensemble significantly decreased when the ellipticity of the excitation light was increased. Considering that the crystal axes of NCs have different polar angles (with respect to the excitation

---

*Corresponding author: hirori@scl.kyoto-u.ac.jp
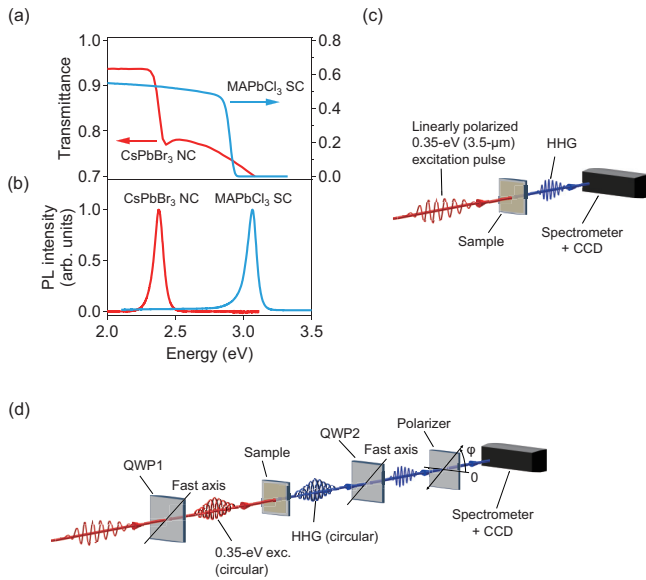†Corresponding author: kanemitu@scl.kyoto-u.ac.jp

FIG. 1. (a) Optical transmission spectra of a $CsPbBr_3$ nanocrystal (NC) film (red) and $MAPbCl_3$ bulk single crystal (SC) (blue). (b) The PL spectra of the $CsPbBr_3$ NC film and the $MAPbCl_3$ SC. (c) Experimental setup for the HHG spectrum measurement using linearly polarized light. (d) Experimental setup for the HHG polarization measurement employing circularly polarized light.

polarization angle), we concluded that the observed reduction in the harmonic intensities was caused by the interference among harmonics emitted from NCs with different phases due to the random crystal-axis orientation.

## II. EXPERIMENT

### A. Sample characterization

The red solid curves in Figs. 1(a) and 1(b) show the transmission and photoluminescence (PL) spectra, respectively, of the $CsPbBr_3$ perovskite NC film. The thin film sample was prepared by drop casting and spin coating the colloidal perovskite NCs (dispersed in hexane) on a sapphire substrate. The NC film exhibits peak structures in the absorption and PL spectra at around 2.38 eV, resulting from the quantum confinement effect in the NC. The band-gap energy of bulk $CsPbBr_3$ is about 2.34 eV [20]. The transmission electron microscope (TEM) image of a close-packed NC film (prepared for the TEM measurement) shows that the NC shape is cubic and the average NC edge length is about 10 nm (see the Appendix). Note that the NCs on the sapphire substrate used for HHG experiment have the same size but are not aligned as in the TEM image. For reference, the transmission and PL spectra of an $MAPbCl_3$ SC with a thickness of 1 mm are shown as the blue curves in Figs. 1(a) and 1(b), respectively. The band-edge exciton PL of the $MAPbCl_3$ SC appears near 3.1 eV. This $MAPbCl_3$ bulk crystal has the same cubic structure as bulk $MAPbBr_3$ at room temperature. Furthermore, owing to its wider band-gap energy, the PL spectrum of the $MAPbCl_3$ SC does not overlap with the HHs in the visible region. Thus, for the comparison between the ellipticity dependencies of the SC and NC samples, bulk $MAPbCl_3$ is appropriate. As shown

in Fig. 1(a), while the bulk material has a sharp absorption onset at the band edge with the relatively strong absorption of $\alpha \sim 10^5 \, cm^{-1}$, [44], the spin coating process of the NCs allowed us to prepare a thin film with an absorption that is much weaker than that of the SC sample. This reduces the reabsorption of HHs by the sample.

### B. Measurement of HHG

A commercial multistage optical parametric amplifier system (Opera from Coherent Inc., driven by a Ti:sapphire laser at a repetition rate of 1 kHz) was used to generate midinfrared excitation laser pulses at a center wavelength of 3.5 $\mu$m, a pulse energy of 60 $\mu$J, and a pulse width of 80 fs. Figure 1(c) describes the experimental setup that uses the linearly polarized midinfrared laser light to observe HHs from the NC film. The excitation spot had a diameter of about 500 $\mu$m. A spectrometer with a charge-coupled device (CCD) camera was used to directly analyze the spectrum of the light emitted from the sample. Figure 1(d) shows the setup that employs circularly polarized excitation light, which allows us to study the dependence of HHs on the ellipticity of the employed excitation light. It enables us to obtain information regarding the crystal symmetry. To determine the dependence of the HH emission intensity on the ellipticity of the excitation light, a quarter waveplate (QWP1) was first used to convert the linear polarization state of the excitation pulse into right-handed (or left-handed) circular polarization. Passing the HHs through another QWP2, the right-handed and left-handed circularly polarized components of the generated HHs were converted into linearly polarized light with a 90° difference. The polarization state of the generated HHs can be determined by analyzing the two components by using a polarizer before the spectrometer.

## III. RESULTS

### A. High-order harmonic spectra obtained using linearly polarized light

Figure 2(a) shows the HH spectra that were obtained from the $CsPbBr_3$ NC film and the $MAPbCl_3$ SC sample under excitation with the linearly polarized light. While the SC sample exhibits HHs only up to the 9th order, the NC sample exhibits relatively strong HHs up to the 13th order. The HHG spectrum of the NC sample extends to the ultraviolet region owing to a weak reabsorption of the HHs. The weak reabsorption is a result of the thin film fabrication by spin coating. We also verified that no HHs were observed from a sapphire substrate that was only coated with the organic ligand, confirming that the spectra shown in Fig. 2(a) are the HHs of the $CsPbBr_3$ NCs.

Figure 2(b) shows the excitation intensity dependencies of the harmonics obtained from the NC film. All the observed data points deviate from the scaling law, and thus, this data indicate that the HHG in this sample is a nonperturbative phenomenon. The HHs of the NC film do not follow the scaling law even at weak excitation intensities, which is in contrast to the results of similar experiments on an $MAPbCl_3$ bulk crystal [39]. This may be a result of the discrete band structure of the $CsPbBr_3$ NCs; one possible explanation is that
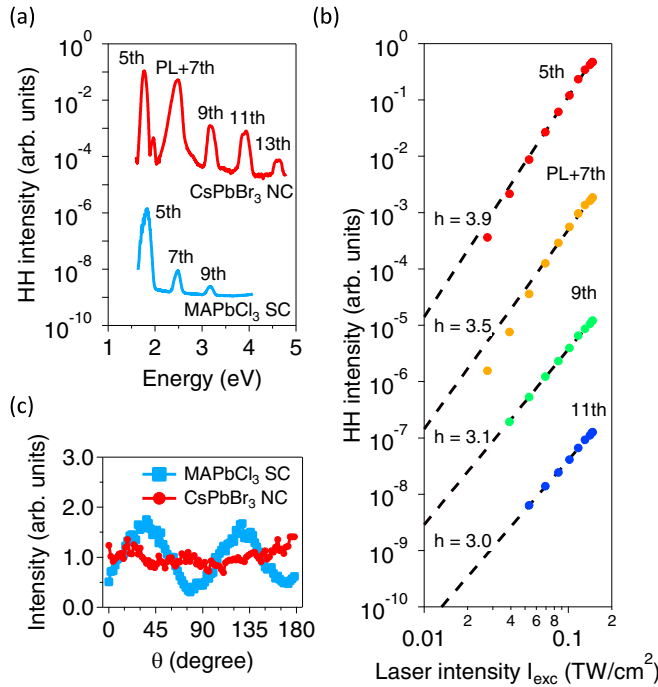
FIG. 2. (a) HH spectra emitted from the $CsPbBr_3$ NC film (red curve) and the $MAPbBr_3$ SC sample (blue curve) under linearly polarized 0.35-eV excitation. (b) Excitation intensity dependencies of the HHs obtained from the $CsPbBr_3$ NC film. The dashed lines are proportional to $I_{exc}^h$ and serve as guides to the eye. (c) The dependence of the 5th harmonic from the $CsPbBr_3$ NC film (red circles) on the polarization angle of excitation pulse and that of the $MAPbCl_3$ SC (blue squares).



FIG. 3. (a) HH spectra of the $CsPbBr_3$ NC film for linearly polarized excitation (blue dashed line) and circularly polarized excitation (red solid line). The data were measured without the polarizer in front of the CCD. (b) Polarization measurement result of the 5th harmonic of a GaSe SC (upper panel) and that of the $CsPbBr_3$ NC film (lower panel). The horizontal axis is the rotation angle $\varphi$ of the polarizer in front of the CCD [Fig. 1(d)]. The colored two-dimensional data visualizes the spectrum of the light of the 5th harmonic that has passed through the polarizer as a function of polarizer angle $\varphi$. (c) The polar graph of the intensity of the 5th harmonic with respect to $\varphi$. The data points shown in the range from 180° to 360° are the same as those shown in (b). (d) Dependencies of the 5th to 13th harmonics of $CsPbBr_3$ NC film on the ellipticity of excitation light. The dependence of the 5th harmonic of $MAPbCl_3$ SC is shown by the dashed black curve and that of PC thin film is shown by the dashed purple curve.

the discrete band structure suppresses the nonlinear excitation of carriers by Pauli blocking and thus leads to a reduced harmonic intensity. (The dependence of the 7th harmonic cannot be evaluated accurately because of the overlap with the PL signal.) At high excitation densities of $0.15 \, TW/cm^2$ (corresponding to electric fields above 11 MV/cm), we found that the harmonic intensity gradually decreased on a time scale of a few minutes. The hysteresis of the excitation intensity dependence was measured, and it was found that the damage threshold of these NCs is about $0.15 \, TW/cm^2$. Therefore, in the following experiments, the excitation intensity was kept below this threshold value.

In Fig. 2(c), we plot the excitation-polarization direction dependence of the 5th harmonic for both the $CsPbBr_3$ NC film (red circles) and the $MAPbCl_3$ SC (blue squares). The intensity of the 5th harmonic was measured as a function of the polarization direction of the linearly polarized pulse, which was changed by a half-wave plate. For the SC sample, we can confirm a fourfold rotational symmetry of the perovskite cubic crystal. On the other hand, the HH intensity from the NC sample is almost uniform. This indicates that the crystal axes of the NCs in the film are randomly oriented. In Fig. 2(a), we note that lack of even-order harmonics from the SC sample can be explained with the inversion symmetry of the perovskite crystal structure [45]. A perfect randomness in the NC orientation within the entire excitation spot does not break
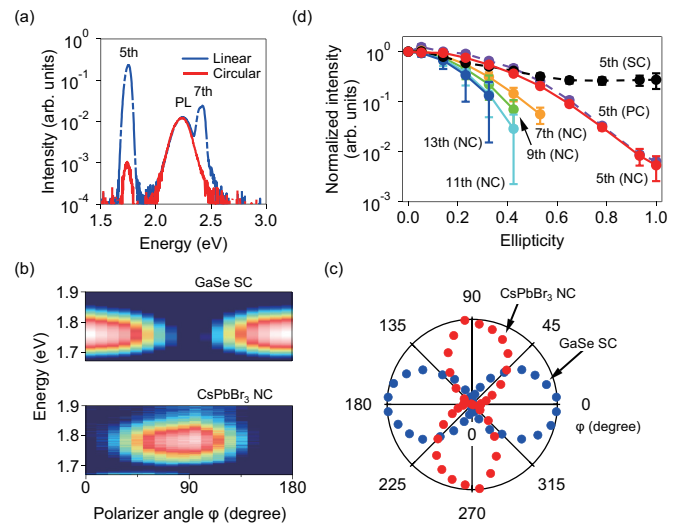
the inversion symmetry and thus also the NC film generates only odd HH components.

## B. Characteristics of high-order harmonic spectra obtained using elliptically polarized light

To examine the selection rule for HHG in this NC film, we compared the HH spectra obtained from the NC film for excitation with circularly and linearly polarized light as shown in Fig. 3(a). While the excitation with linearly polarized light provides the spectra of 5th and 7th harmonics in this spectral window (blue solid curve), only the 5th harmonic can be confirmed for the circular polarization even at the same excitation intensity (red solid curve). Figure 3(b) shows the spectra of the 5th harmonic for the $CsPbBr_3$ NC film (lower panel) and a GaSe SC (upper panel) as a function of the rotation angle $\varphi$ of the polarizer in front of the CCD camera. Figure 3(c) shows the corresponding polar plots. GaSe serves as a reference material in this work, because the circular polarization selection rule of its hexagonal crystal structure has been studied well, which allows us to confirm the reliability of our experimental setup [46–48]. The blue data in Fig. 3(c) show that the excitation with the right-handed circularly polarized light causes the emission of the 5th harmonic with a left-handed circular polarization from the (0001)-oriented GaSe SC. These data

are consistent with the selection rule of HHG for the threefold rotational symmetry of GaSe [48]. On the other hand, the red data in Fig. 3(c) show that the 5th harmonic of the perovskite NC film exhibits a right-handed circular polarization for the right-handed circular excitation. As the crystal structure of the perovskite NCs is cubic with a fourfold rotational symmetry [20], the fact that the polarization of the emitted 5th harmonic equals the excitation polarization is consistent with the selection rule for this crystal structure [39]. This confirms that the randomness in the NC orientation has no influence on the selection rule.

To identify the mechanism of the decrease in the HH intensity under circularly polarized light, we measured the dependence of the HH intensity on the ellipticity of the excitation light. Figure 3(d) shows the excitation-ellipticity dependencies of the HHs for the CsPbBr$_3$ NC sample, the MAPbCl$_3$ SC sample, and a polycrystalline (PC) MAPbCl$_3$ thin film sample. Here, we used no polarizer in front of the CCD. The ellipticity of the excitation light was changed from 0 (linear polarization) to 1 (circular polarization). It can be confirmed that the HH intensities of all three samples decrease as the ellipticity increases. However, the reduction in the HH intensity emitted from the NC film for circular polarization is much larger than that observed for the SC sample. Additionally, the HH intensities of the NC film fall faster as the harmonic order increases, despite the higher exponent of the power law [h in Fig. 2(b)] for lower orders. While we can expect that the HH intensities decrease because the peak electric field applied to the sample decreases when the ellipticity is changed from 0 to 1, the behavior of the NC film contains an additional effect. The fact that the PC sample exhibited a trend that is very similar to that of the NC film suggests that the crystal orientation is involved.

## IV. DISCUSSION

The significant reduction in the HH intensities from the NC film under excitation with circularly polarized light suggests destructive interference among HHs emitted from NCs with different phases. Such a phase difference can occur because the NCs in the film have different tilting angles. To quantify the interference effect, the $n$ th-order harmonic's electric field of a single NC, $E_{NC,nth}(t)$, has to be formulated. The electric field $\boldsymbol{E}(t)$ of the excitation pulse with circular polarization can be described by

$$E(t) = \begin{pmatrix} E_x(t) \\ E_y(t) \end{pmatrix} = E_0 \begin{pmatrix} \cos(\omega t) \\ \sin(\omega t) \end{pmatrix}, \tag{1}$$

where $E_0$ is the electric field amplitude and $\omega$ is the angular frequency. To distinguish the different NCs in an ensemble, we assign a different label to each NC. The electric field of the $n$ th-order harmonic from the NC labeled "$A$" can then be described by

$$E_{A,nth}(t) = \begin{pmatrix} E_{A,nth,x}(t) \\ E_{A,nth,y}(t) \end{pmatrix} = E_{0,nth,R} \begin{pmatrix} \cos(n\omega t + \delta_R) \\ \sin(n\omega t + \delta_R) \end{pmatrix} + E_{0,nth,L} \begin{pmatrix} \cos(-n\omega t + \delta_L) \\ \sin(-n\omega t + \delta_L) \end{pmatrix}, \tag{2}$$

where $E_{0,nth,R}$ and $E_{0,nth,L}$ represent the amplitudes of the right- and left-handed circularly polarized components. $\delta_R$ and $\delta_L$ are the phase shifts of the two components. Furthermore, we consider another NC labeled "$B$" that has a crystal tilt angle $\theta$ relative to $A$. The electric field of the $n$th-order harmonic of $B$ equals that from $A$ including a shift in time $(-\theta/\omega)$ as follows:

$$E_{B,nth}(t,\theta) = \begin{pmatrix} E_{B,nth,x}(t,\theta) \\ E_{B,nth,y}(t,\theta) \end{pmatrix} = \begin{pmatrix} \cos(\theta) & -\sin(\theta) \\ \sin(\theta) & \cos(\theta) \end{pmatrix} \begin{pmatrix} E_{A,nth,x}\left(t - \frac{\theta}{\omega}\right) \\ E_{A,nth,y}\left(t - \frac{\theta}{\omega}\right) \end{pmatrix}$$

$$= E_{0,nth,R} \begin{pmatrix} \cos\left(n\omega\left(t - \frac{\theta}{\omega}\right) + \theta + \delta_R\right) \\ \sin\left(n\omega\left(t - \frac{\theta}{\omega}\right) + \theta + \delta_R\right) \end{pmatrix} + E_{0,nth,L} \begin{pmatrix} \cos\left(-n\omega\left(t - \frac{\theta}{\omega}\right) + \theta + \delta_L\right) \\ \sin\left(-n\omega\left(t - \frac{\theta}{\omega}\right) + \theta + \delta_L\right) \end{pmatrix}. \tag{3}$$

The time-dependent electric field $E_{all,nth}(t)$ of the $n$ th-order harmonic from the ensemble of NCs can be obtained by integration,

$$E_{all,nth}(t) = \int_0^{2\pi} \rho(\theta) E_{B,nth}(t,\theta) d\theta. \tag{4}$$

Here, $\rho(\theta)$ is the number density of NCs that are tilted by an angle $\theta$. If we assume perfect randomness, $\rho(\theta)$ is constant. By using Eqs. (3) and (4), we find that $E_{all,nth}(t)$ becomes zero in this case. This cancellation of the generated HH intensity is a consequence of the interference among the HHs emitted from NCs with random phases. Moreover, Eq. (3) shows that the changes in the phase become more rapid as the harmonic order $n$ increases. The cancellation effect is more pronounced for higher orders because these HHs are more sensitive to

the tilting angle $\theta$, which is consistent with the data shown in Fig. 3(d). Hence, we found that we can control the HH intensities by simply changing the excitation ellipticity.

Finally, we note that Eq. (3) can only be applied in the case of circularly polarized waves (i.e., it cannot be used to predict the ellipticity dependence). However, Eq. (3) can be used to discuss the effect of the degree of randomness, because the HH intensity predicted for circularly polarized excitation can be changed to any value by selecting an appropriately normalized function $\rho(\theta)$. For example, the nonzero HH intensity of the NC film under the circularly polarized excitation condition in Fig. 3(d) may indicate that $\rho(\theta)$ is not constant (i.e., this is not a perfectly random sample). Another possible explanation is that the excitation light used in this experiment was actually slightly elliptical (we experimentally confirmed a small difference within $\pm 5\%$).
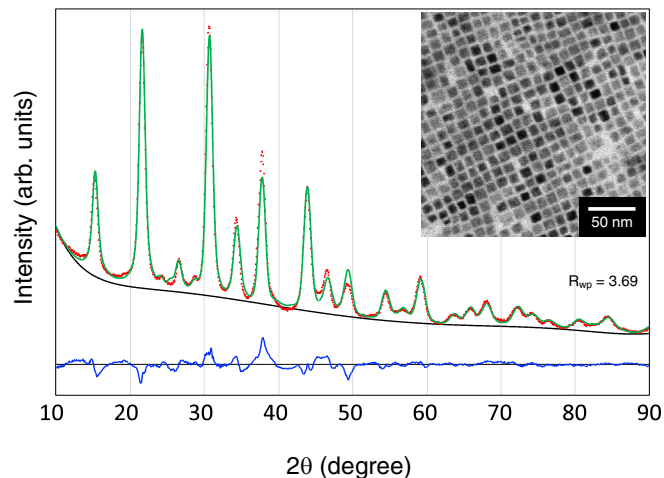
FIG. 4. XRD pattern of the $CsPbBr_3$ NCs with a size of 9.5 $\pm$ 0.8 nm. The figure plots the observed (red dots), calculated (green line), and background (black line) profiles after Rietveld refinement. The difference between the observed and calculated profiles is shown by the blue curve. The TEM image is shown in the inset.

## V. CONCLUSION

In conclusion, we have shown that excitation of a perovskite NC film with strong 3.5-$\mu$m midinfrared light results in generation of HHs up to the 13th order. It was confirmed that the polarization of the 5th harmonic observed under excitation with circularly polarized light satisfies the selection rule of the fourfold rotational symmetry of the perovskite crystal structure. We also discussed the random-phase-induced cancellation effect that occurs in the case of excitation with circularly polarized light and clarified that the random crystal axis of NC causes a significant reduction in the emitted HH intensity. Our observation of HHs from a NC film under excitation with elliptic light has shown that the crystal-axis orientation of the NCs is an important factor for the development of an optical intensity modulator for HHs with a broad spectral range.

## ACKNOWLEDGMENT

## APPENDIX: SAMPLE SYNTHESIS AND CHARACTERIZATION

The $CsPbBr_3$ NCs with an average edge length of 9.5 $\pm$ 0.8 nm (inset of Fig. 4) were synthesized under an anhydrous condition with a slight modification to the rapid hot-injection method reported in the literature [20,23]. The outline of the procedure is as follows: $Cs_2CO_3$ (160 mg), oleic acid (0.5 mL), and 1-octadecene (6 mL) were mixed and heated to 160 °C under a nitrogen atmosphere to form a Cs-oleate solution. In addition, a mixture of $PbBr_2$ (690 mg), oleic acid (5 mL), oleylamine (5 mL), and 1-octadecene (50 mL) was degassed in vacuum for 1 h at 100 °C. After this mixture was heated to 180 °C under a nitrogen atmosphere, 4 mL of the Cs-oleate solution, that had been kept at 160 °C, was rapidly injected under vigorous stirring. The reaction solution was held at 180 °C for 5 min and then quenched in a water bath to room temperature. Purification and size selection of the obtained polydisperse $CsPbBr_3$ NCs were achieved by precipitation fractionation with centrifugation in *n*-hexane.

The NC size was investigated using a transmission electron microscope (TEM, JEM-1011 from JEOL Ltd., which was operated at an acceleration voltage of 100 kV). The sample for the TEM observation was prepared by drop casting the $CsPbBr_3$ NC solution onto a carbon-coated copper grid and drying in ambient conditions. The x-ray diffraction pattern of the $CsPbBr_3$ NCs was obtained using a powder x-ray diffractometer (XRD, X'Pert Pro MPD from PANalytical Ltd., Ni-filtered Cu-$K\alpha$ radiation generated at 45 kV and 40 mA). The sample for the XRD measurement was prepared by depositing the $CsPbBr_3$ NCs on a synthetic silica glass substrate with dimensions of $10 \times 10 \times 0.5$ mm. A quantitative phase analysis based on Rietveld refinement (Fig. 4) revealed that 81 wt % of our $CsPbBr_3$ NCs were in the cubic phase (space group of $Pm\bar{3}m$) and 19 wt % were in the orthorhombic phase (space group of *Pbnm*). Although the orthorhombic crystals affect the polarization selection rule and excitation ellipticity dependence in Fig. 3, in the text, we neglected the orthorhombic NCs due to the reasons explained below.

Regarding the circular polarization selection rule, on average, 81% of the particles are cubic NCs, and thus the 5th-order selection rule for the fourfold rotational symmetry should predominate. The remaining 19% of the crystals are orthorhombic. However, since the three lattice constants of the presently considered orthorhombic crystal structure have almost the same length, the selection rule should be almost the same as that of the cubic crystal. Hence we consider that there is almost no left-handed circularly polarized component.

[1] S. D. Stranks and H. J. Snaith, Nat. Nanotechnol. **10**, 391 (2015).

[2] B. R. Sutherland and E. H. Sargent, Nat. Photon. **10**, 295 (2016).

[3] Y. Kanemitsu, J. Mater. Chem. C **5**, 3427 (2017).

[4] A. Kojima, K. Teshima, Y. Shirai, and T. Miyasaka, J. Am. Chem. Soc. **131**, 6050 (2009).

[5] M. M. Lee, J. Teuscher, T. Miyasaka, T. N. Murakami, and H. J. Snaith, Science **338**, 643 (2012).

[6] Z.-K. Tan, R. S. Moghaddam, M. L. Lai, P. Docampo, R. Higler, F. Deschler, M. Price, A. Sadhanala, L. M. Pazos, D. Credgington, F. Hanusch, T. Bein, H. J. Snaith, and R. H. Friend, Nat. Nanotechnol. **9**, 687 (2014).

[7] G. Xing, N. Mathews, S. S. Lim, N. Yantara, X. Liu, D. Sabba, M. Grätzel, S. Mhaisalkar, and T. C. Sum, Nat. Mater. **13**, 476 (2014).

[8] L. Dou, Y. M. Yang, J. You, Z. Hong, W.-H. Chang, G. Li, and Y. Yang, Nat. Commun. **5**, 5404 (2014).

[9] S. Yakunin, M. Sytnyk, D. Kriegner, S. Shrestha, M. Richter, G. J. Matt, H. Azimi, C. J. Brabec, J. Stangl, M. V. Kovalenko, and W. Heiss, Nat. Photonics **9**, 444 (2015).

[10] H. Tahara, T. Aharen, A. Wakamiya, and Y. Kanemitsu, Adv. Opt. Mater. **6**, 1701366 (2018).

[11] S. Yakunin, B. M. Benin, Y. Shynkarenko, O. Nazarenko, M. I. Bodnarchuk, D. N. Dirin, C. Hofer, S. Cattaneo, and M. V. Kovalenko, Nat. Mater. **18**, 846 (2019).

[12] T. Handa, H. Tahara, T. Aharen, and Y. Kanemitsu, Sci. Adv. **5**, eaax0786 (2019).

[13] H. Utzat, W. Sun, A. E. Kaplan, F. Krieg, M. Ginterseder, B. Spokoyny, N. D. Klein, K. E. Shulenberger, C. F. Perkinson, M. V. Kovalenko, and M. G. Bawendi, Science **363**, 1068 (2019).

[14] S. D. Stranks, G. E. Eperon, G. Grancini, C. Menelaou, M. J. P. Alcocer, T. Leijtens, L. M. Herz, A. Petrozza, and H. J. Snaith, Science **342**, 341 (2013).

[15] G. Xing, N. Mathews, S. Sun, S. S. Lim, Y. M. Lam, M. Grätzel, S. Mhaisalkar, and T. C. Sum, Science **342**, 344 (2013).

[16] Y. Yamada, T. Nakamura, M. Endo, A. Wakamiya, and Y. Kanemitsu, J. Am. Chem. Soc. **136**, 11610 (2014).

[17] S. D. Stranks, V. M. Burlakov, T. Leijtens, J. M. Ball, A. Goriely, and H. J. Snaith, Phys. Rev. Appl. **2**, 034007 (2014).

[18] Y. Yamada, T. Yamada, L. Q. Phuong, N. Maruyama, H. Nishimura, A. Wakamiya, Y. Murata, and Y. Kanemitsu, J. Am. Chem. Soc. **137**, 10456 (2015).

[19] A. M. A. Leguy, P. Azarhoosh, M. I. Alonso, M. Campoy-Quiles, O. J. Weber, J. Yao, D. Bryant, M. T. Weller, J. Nelson, A. Walsh, M. van Schilfgaarde, and P. R. F. Barnes, Nanoscale **8**, 6317 (2016).

[20] L. Protesescu, S. Yakunin, M. I. Bodnarchuk, F. Krieg, R. Caputo, C. H. Hendon, R. X. Yang, A. Walsh, and M. V. Kovalenko, Nano Lett. **15**, 3692 (2015).

[21] Q. A. Akkerman, G. Rainò, M. V. Kovalenko, and L. Manna, Nat. Mater. **17**, 394 (2018).

[22] N. S. Makarov, S. Guo, O. Isaienko, W. Liu, I. Robel, and V. I. Klimov, Nano Lett. **16**, 2349 (2016).

[23] N. Yarita, H. Tahara, T. Ihara, T. Kawawaki, R. Sato, M. Saruyama, T. Teranishi, and Y. Kanemitsu, J. Phys. Chem. Lett. **8**, 1413 (2017).

[24] M. A. Becker, R. Vaxenburg, G. Nedelcu, P. C. Sercel, A. Shabaev, M. J. Mehl, J. G. Michopoulos, S. G. Lambrakos, N. Bernstein, J. L. Lyons, T. Stöferle, R. F. Mahrt, M.V. Kovalenko, D. J. Norris, G. Rainò, and A. L. Efros, Nature (London) **553**, 189 (2018).

[25] P. Tamarat, M. I. Bodnarchuk, J. B. Trebbia, R. Erni, M. V. Kovalenko, J. Even, and B. Lounis, Nat. Mater. **18**, 717 (2019).

[26] G. Rainò, M. A. Becker, M. I. Bodnarchuk, R. F. Mahrt, M. V. Kovalenko, and T. Stöferle, Nature (London) **563**, 671 (2018).

[27] K. Ohara, T. Yamada, H. Tahara, T. Aharen, H. Hirori, H. Suzuura, and Y. Kanemitsu, Phys. Rev. Mater. **3**, 111601(R) (2019).

[28] E. Kobiyama, H. Tahara, R. Sato, M. Saruyama, T. Teranishi, and Y. Kanemitsu, Nano Lett. **20**, 3905 (2020).

[29] P. B. Corkum, Phys. Rev. Lett. **71**, 1994 (1993).

[30] P. B. Corkum and F. Krausz, Nat. Phys. **3**, 381 (2007).

[31] A. McPherson, G. Gibson, H. Jara, U. Johann, T. S. Luk, I. A. McIntyre, K. Boyer, and C. K. Rhodes, J. Opt. Soc. Am. B **4**, 595 (1987).

[32] S. Ghimire, A. D. DiChiara, E. Sistrunk, P. Agostini, L. F. DiMauro, and D. A. Reis, Nat. Phys. **7**, 138 (2011).

[33] O. Schubert, M. Hohenleutner, F. Langer, B. Urbanek, C. Lange, U. Huttner, D. Golde, T. Meier, M. Kira, S. W. Koch, and R. Huber, Nat. Photon. **8**, 119 (2014).

[34] Y. S. You, Y. Yin, Y. Wu, A. Chew, X. Ren, F. Zhuang, S. Gholam-Mizaei, M. Chini, Z. Chang, and S. Ghimire, Nat. Commun. **8**, 724 (2017).

[35] H. Liu, Y. Li, Y. S. You, S. Ghimire, T. F. Heinz, and D. A. Reis, Nat. Phys. **13**, 262 (2017).

[36] N. Yoshikawa, T. Tamaya, and K. Tanaka, Science **356**, 736 (2017).

[37] H. Hirori, P. Xia, Y. Shinohara, T. Otobe, Y. Sanari, H. Tahara, N. Ishii, J. Itatani, K. L. Ishikawa, T. Aharen, M. Ozaki, A. Wakamiya, and Y. Kanemitsu, APL Mater. **7**, 041107 (2019).

[38] Y. S. You, D. A. Reis, and S. Ghimire, Nat. Phys. **13**, 345 (2017).

[39] Y. Sanari, H. Hirori, T. Aharen, H. Tahara, Y. Shinohara, K. L. Ishikawa, T. Otobe, P. Xia, N. Ishii, J. Itatani, S. A. Sato, and Y. Kanemitsu, Phys. Rev. B **102**, 041125(R) (2020).

[40] Y. Sanari, T. Otobe, Y. Kanemitsu, and H. Hirori, Nat. Commun. **11**, 3069 (2020).

[41] L. E. Brus, J. Chem. Phys. **80**, 4403 (1984).

[42] A. I. Ekimov, A. L. Efros, and A. A. Onushchenko, Solid State Commun. **56**, 921 (1985).

[43] Y. Kanemitsu, Phys. Rep. **263**, 1 (1995).

[44] T. Yamada, T. Aharen, and Y. Kanemitsu, Phys. Rev. Lett. **120**, 057404 (2018).

[45] R. W. Boyd, *Nonlinear Optics* (Academic, New York, 1994).

[46] C. L. Tang and H. Rabin, Phys. Rev. B **3**, 4025 (1971).

[47] O. E. Alon, V. Averbukh, and N. Moiseyev, Phys. Rev. Lett. **80**, 3743 (1998).

[48] N. Saito, P. Xia, F. Lu, T. Kanai, J. Itatani, and N. Ishii, Optica **4**, 1333 (2017).